Metallaborane Reactivity. Complexities of Cobalt Carbonyl Fragment Addition to 1,2-{Cp*RuH}$_2$B$_3$H$_7$, Cp* = η^5-C$_5$Me$_5$, and Characterization of a Diruthenium Analogue of Pentaborane(11) 1,2-{Cp*Ru}$_2$(CO)$_2$B$_3$H$_7$

Antonio DiPasquale,† Xinjian Lei, and Thomas P. Fehlner*

Department of Chemistry and Biochemistry, University of Notre Dame, Notre Dame, Indiana 46556-5670

Received July 2, 2001

The reaction of 1,2-{Cp*RuH}$_2$B$_3$H$_7$ (**1**), Cp* = η^5-C$_5$Me$_5$, with Co$_2$(CO)$_8$ in hexane yields two major ruthenaborane products, nido-1,2-{Cp*RuH}$_2$-3-Co(CO)$_4$B$_3$H$_4$ (**2**) and arachno-{Cp*RuH}(CO)B$_3$H$_7$ (**3**), as well as two other ruthenaboranes in low yield. In toluene, benzene, and THF one of these minor ruthenaborane products is found with an enhanced yield intermediate between those of **2** and **3**. This compound has been isolated and characterized in solution and the solid state as the 8 skeletal electron pair (sep) arachno 1,2-{Cp*Ru}$_2$(CO)$_2$B$_3$H$_7$ (**4**) and shown to convert into a second isomeric form of similar stability. One isomer constitutes a diruthenium analogue of 8-sep pentaborane(11), whereas the other mimics the geometry of a known metal cluster with 8 sep. The variation in product concentrations in benzene, including [Cp*Ru(CO)$_2$]$_2$, {Cp*Ru(CO)$_2$}Co(CO)$_4$, and HCo(CO)$_4$, as a function of time and Co$_2$(CO)$_8$/**1** ratio has been determined by ^{1}H and ^{11}B NMR spectroscopy and interpreted in terms of a reaction pathway featuring competitive Co(CO)$_4$ radical addition to ruthenium to yield **2** plus **3** and to boron to yield **4**. The apparent solvent dependence of product distribution is attributed to impurity-initiated decomposition of the boron-based radical in hexane.

Introduction

The structural side of metallaborane chemistry[1,2] contains a rich array of compounds closely related to boranes on one hand and metal clusters on the other.[3] Some are isoelectronic with metal−hydrocarbyl complexes of organometallic chemistry,[4] and some display unprecedented cluster shapes that reveal unique properties of compounds containing direct transition metal−boron bonds.[5,6] In contrast to, for example, organometallic chemistry, but with some exceptions,[7,8] our knowledge of the characteristic reactivities associated with metallaboranes is in a more rudimentary state. In part, this is due to a lack of efficient routes to pure starting materials, which would permit surveys of reactivity of sufficient breadth to be meaningful. With the discovery that the reaction of monocyclopentadienylmetal halides with monoboranes constitutes a convenient, general route to one class of metallaboranes,[9,10] development of the reactivity of metallaboranes now has become possible.

In an ongoing effort to access the broad trends in the reactivity of metallaboranes containing a range of transition metal atoms, we have examined thermolysis reactions and reactions with metal fragments, monoboranes, and Lewis bases, e.g., CO.[11−13] The reactivity of 1,2-{Cp*RuH}$_2$B$_3$H$_7$ (**1**), Cp* = η^5-C$_5$Me$_5$, has also been explored by others.[10,14−16] As Co$_2$(CO)$_8$ is often used as a general source of Co(CO)$_x$ fragments by cluster chemists,[17] we have examined its reactivity with metallaboranes containing metals from groups 6−9.[9,18] In the case of **1**, competitive cobalt fragment addition and ruthenium fragment elimination were observed as well as a minor product of fascinating composition and structure.[19] Hence, we set out to explore mechanistic aspects of this reaction in order to try to optimize this interesting product as well as to obtain more detailed information on the origin of all products. In the reaction, the isolation of a fourth metallaborane product in good yield was achieved even though the yields of the minor

† Undergraduate research participant.

(1) Kennedy, J. D. *Prog. Inorg. Chem.* **1984**, *32*, 519.
(2) Kennedy, J. D. *Prog. Inorg. Chem.* **1986**, *34*, 211.
(3) Wade, K. *Adv. Inorg. Chem. Radiochem.* **1976**, *18*, 1.
(4) Grimes, R. N. *Acc. Chem. Res.* **1978**, *11*, 420.
(5) Ghosh, S.; Shang, M.; Li, Y.; Fehlner, T. P. *Angew. Chem., Int. Ed.* **2001**, *40*, 1125.
(6) Fehlner, T. P. *Struct. Bonding* **1997**, *87*, 112.
(7) Jan, D.-Y.; Shore, S. G. *Organometallics* **1987**, *6*, 428.
(8) Jan, D.-Y.; Workman, D. P.; Hsu, L.-Y.; Krause, J. A.; Shore, S. G. *Inorg. Chem.* **1992**, *31*, 5123.
(9) Fehlner, T. P. *Organometallics* **2000**, *19*, 2643.
(10) Kawano, Y.; Matsumoto, H.; Shimoi, M. *Chem. Lett.* **1999**, 489.
(11) Lei, X.; Shang, M.; Fehlner, T. P. *J. Am. Chem. Soc.* **1999**, *121*, 1275.
(12) Lei, X.; Shang, M.; Fehlner, T. P. *Chem. A Eur. J.* **2000**, *6*, 2653.
(13) Lei, X.; Shang, M.; Fehlner, T. P. *Organometallics* **2000**, *19*, 5266.
(14) Kawano, Y.; Shimoi, M. *Chem. Lett.* **1998**, 935.
(15) Pangan, L. N.; Kawano, Y.; Shimoi, M. *Organometallics* **2000**, *19*, 5575.
(16) Pangan, L. N.; Kawano, Y.; Shimoi, M. *Inorg. Chem.* **2001**, *40*, 1985.
(17) *The Chemistry of Metal Cluster Complexes*; Shriver, D. F., Kaesz, H. D., Adams, R. D., Eds.; VCH: New York, 1990.
(18) Fehlner, T. P. *J. Chem. Soc., Dalton Trans.* **1998**, 1525.
(19) Lei, X.; Shang, M.; Fehlner, T. P. *Angew. Chem., Int. Ed.* **1999**, *38*, 1986.

10.1021/om010589q CCC: $20.00
Publication on Web 10/19/2001

Chart 1

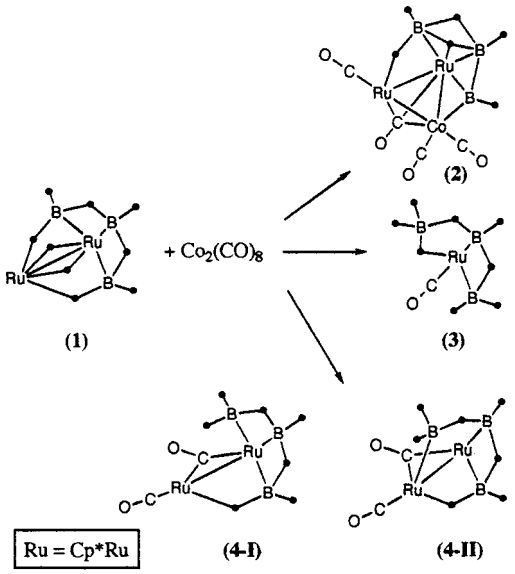

product of initial interest could not be significantly enhanced. Mechanistic complexity and the sensitivity of the system to conditions largely frustrated achievement of the second objective, but some significant, qualitative characteristics of the reaction pathway were defined. The dependence of the product distribution of a reaction with $Co_2(CO)_8$ makes an intercomparison of metallaborane reactivities based on product types less informative for this fragment source.

Results and Discussion

As illustrated in Chart 1, in the earlier study the principal metallaboranes isolated from the reaction of $Co_2(CO)_8$ with **1** were nido-1,2-{Cp*RuH}$_2$-3-Co(CO)$_4$B$_3$H$_4$ (**2**) and arachno-{Cp*RuH}(CO)B$_3$H$_7$ (**3**), with the relative yield of the latter being enhanced at low $Co_2(CO)_8$/**1** ratios.[11] In addition, tiny yields of {Cp*$_2$Ru$_2$B$_4$H$_{10}$}$_2$Ru were isolated from the reaction mixture.[19] Non-boron-containing products identified were [Cp*Ru(CO)$_2$]$_2$, {Cp*Ru(CO)$_2$}Co(CO)$_4$, HCo(CO)$_4$, and Co$_4$(CO)$_{12}$. For the new work, ^{1}H and ^{11}B NMR was chosen to examine the time and concentration dependence of the reaction composition; hence, reactions were carried out in C_6D_6 as solvent rather than hexane, which was used previously. Although both **2** and **3** were still observed as products, a new product was observed in disconcertingly high yield. Examination of earlier spectroscopic data showed its presence in ≈10-fold lower abundance. This unexpected solvent dependence was confirmed (see below), but characterization of this new product as well as a non-boron-containing product must be presented before an analysis of the reaction itself.

Isolation and Characterization of 1,2-{Cp*Ru}$_2$-(CO)$_2$B$_3$H$_7$ (4). With optimal stoichiometry and reaction time, the reaction mixture was subjected to the chromatographic procedure described in the Experimental Section. A pure sample (**4-I**) was characterized spectroscopically; however, it did not remain pure but rather partially converted into an isomeric form (**4-II**) and, eventually, decomposed entirely. [Cp*Ru(CO)$_2$]$_2$ is one of the decomposition products. Complete conversion was not achieved before significant decomposition occurred. Hence, although the two forms must have similar stabilities, the more stable of the two is not known. The second isomeric form was also present in low amounts in the reaction mixture. To further complicate matters, single crystals that were obtained produced a solid-state structure attributable to either **4-I** or **4-II**. Consequently, every detail of **4-I** and **4-II** is not known; however, the overall compositions and structures are clear.

The description of **4-I** is given first, as spectra of pure **4-II** have not been obtained. The mass spectrum is consistent with the composition {Cp*Ru}$_2$(CO)$_2$B$_3$H$_7$, and the presence of bridging and terminal metal-bound CO ligands is evident in the IR spectrum. The ^{11}B spectrum exhibits two signals of area 1:2. The first is a doublet, whereas the second is best characterized as a multiplet with components of ≈1:4:3 intensity ratio, which could result from a triplet superimposed on a doublet with slightly different chemical shifts (the decoupled spectrum shows a single broad resonance). The ^{1}H NMR spectrum shows two Cp* resonances (inequivalent metal centers), three high-field resonances (−1.7, BHB, −4.7, BHB, and −12.0, BHRu), and four terminal hydrogens ({^{11}B}) in the ratio 1:2:1. A ^{11}B/^{1}H HETCOR experiment showed the boron exhibiting the low-field resonance coupled only to one terminal proton and the BHRu proton at highest field. The two borons at similar chemical shift at higher field show coupling to the other five protons. The ^{13}C NMR shows two inequivalent Cp* ligands but only a single type of CO, indicating the existence of a fluxional process making the bridging and terminal CO ligands equivalent on the NMR time scale without making the Cp* ligands equivalent. Variable-temperature ^{1}H NMR (to −80 °C) shows thermal decoupling of ^{11}B but no evidence of the loss of fluxional motion associated with the framework. Curiously, the lower field Cp* resonance splits into two unequal resonances ($\Delta\delta = 0.06$) at the lowest temperature, perhaps suggesting hindered rotation associated with slowing of the CO exchange.

The molecular formula generates a skeletal electron pair (sep) count of 8, suggesting an arachno structure based on B_5H_{11}. With two heteroatoms 15 structural isomers can be derived from a pentagonal bipyramid by removing two vertexes. Even though many are eliminated by the data, it is not possible to give a most probable structure without first considering its isomer and the crystallographic results.

^{1}H NMR study of the isomerization of **4-I** shows a decrease in the δ −12.0 resonance and a concomitant increase in a single resonance at −11.4 as **4-II** is produced. At the same time a slightly shifted pair of Cp* resonances grows in and the intensity of the pair of Cp* resonances of **4-I** decreases. However, the intensities of the signals at −1.7 and −4.7 remain constant. In the ^{11}B{^{1}H} NMR the signal of intensity 1 at δ 36.7 decreases and one at 29.9 grows in. At the same time the high-field signal of intensity 2 splits into two distinct resonances of approximate intensity 1 each. The ratio of −12.0/−11.4 in the ^{1}H NMR tracks that of 36.7/29.9 in the ^{11}B NMR as a function of time. In Figure 1 a comparison of the intensities of the BHRu resonances relative to that of the BHB signal at −1.7 illustrates the inverse relationship. A terminal and

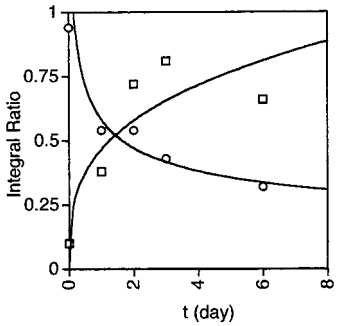

Figure 1. Plot of the ratios of the integrals of the ^{1}H NMR resonances at δ −11.4 (squares) and −12.0 (circles) to that at −1.7 for **4**.

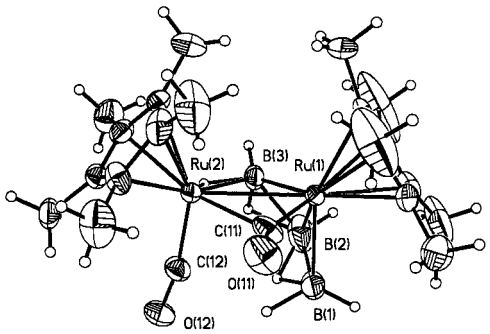

Figure 2. Molecular structure of 1,2-{Cp*Ru}$_2$(CO)$_2$B$_3$H$_7$ (**4**) in the solid state. Selected distances (Å) and angles (deg): Ru(1)−C(11) 1.900(9), Ru(1)−B(2) 2.122(14), Ru(1)−B(3) 2.133(11), Ru(1)−B(1) 2.214(12), Ru(1)−Ru(2) 2.8747(9), Ru(2)−C(12) 1.850(10), Ru(2)−C(11) 2.268(11), Ru(2)−B(3) 2.273(11), B(1)−B(2) 1.75(2), B(2)−B(3) 1.82(2), O(11)−C(11), 1.159(11), O(12)−C(12) 1.145(11), C(11)−Ru(1)−B(2) 112.1(6), C(11)−Ru(1)−B(3)101.7(4), B(2)−Ru(1)−B(3) 50.7(6), C(11)−Ru(1)−B(1) 78.9(5), B(2)−Ru(1)−B(1) 47.4(6), B(3)−Ru(1)−B(1) 89.0(5), C(11)−Ru(1)−Ru(2) 52.0(3), B(2)−Ru(1)−Ru(2) 86.4(4), B(3)−Ru(1)−Ru(2) 51.4(3), B(1)−Ru(1)−Ru(2) 91.4(3), B(2)−B(1)−Ru(1) 63.5(6), B(1)−B(2)−B(3) 117.3(10), B(1)−B(2)−Ru(1) 69.1(7), B(3)−B(2)−Ru(1) 65.0(6), B(2)−B(3)−Ru(1) 64.4(6), B(2)−B(3)−Ru(2) 115.1(8), Ru(1)−B(3)−Ru(2) 81.4(4), B(5)−B(4)−Ru(4) 64.1(5), B(4)−B(5)−B(6) 113.5(8), O(11)−C(11)−Ru(1) 150.1(10), O(11)−C(11)−Ru(2) 22.8(9), Ru(1)−C(11)−Ru(2) 86.7(4), O(12)−C(12)−Ru(2) 167.7(9).

bridging CO absorption with lower frequencies than those of **4-I** are observed in the IR. Thus, the number of metal, boron, and hydrogen atoms remain the same, and considering the close similarity of the chemical shifts, the structures of **4-I** and **4-II** must be very closely related indeed.

The molecular structure resulting from crystals derived from a solution of **4** is shown in Figure 2. As a ^{1}H NMR spectrum of the crystals (but not the crystal used in the diffraction study) showed them to be 90% **4-I** and 10% **4-II**, the structure is attributed to **4-I** even though it could be that of **4-II**. The structure corresponds exactly to what one expects for an 8-sep, five-fragment cluster (arachno). As shown in Chart 2, opening a basal edge of a nido square pyramidal cluster generates the observed structure (a) if the metal fragments are placed in the 1 and 2 positions, as shown from a different perspective in the sketch at the bottom of the chart. The observed structural parameters are within the normal limits for ruthenaboranes. The solid-state structure is consistent with the spectroscopic data assuming the CO

Chart 2

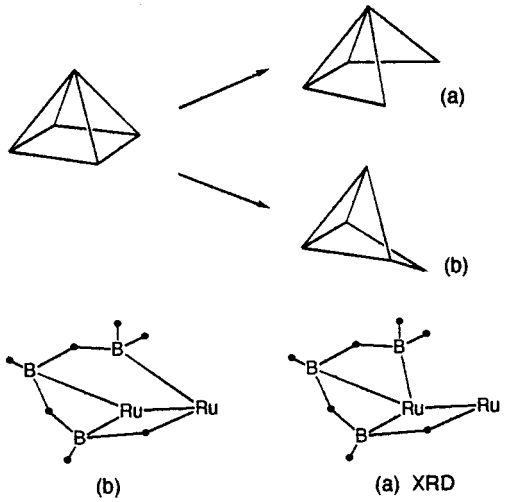

ligands are fluxional on the NMR time scale. **4** constitutes the first example of a characterization of an arachno dimetallapentaborane, although structures of arachno monometallapentaboranes are known.[20]

The next question is, if the solid-state structure is that of **4-I**, what is the structure of **4-II**? Of all the other possible geometric isomers, only that generated by opening a basal-apical edge of a nido square pyramidal cluster, (b) in Chart 2, has the same metal−metal, boron−boron, and metal−boron connectivities as structure (a). Alternatively, this geometry can be generated from a pentagonal bipyramid by removal of two nonadjacent equatorial edges. Furthermore, as shown in the sketch at the bottom, the environments of the boron atoms and their hydrogens (b) are virtually unchanged from those in (a)—the only difference is the metal to which the BH_2 group is attached. B(3) is assigned the low-field ^{11}B resonance which shifts on isomerization, and it is coupled to the high-field BHRu proton (which also shifts) as well as to one terminal proton. The fact that coupling to the adjacent BHB proton is not observed is unusual but not unprecedented, as bridging hydrogens need not be symmetrically placed between two inequivalent boron sites, e.g., in B_4H_{10}, which this particular interaction can be seen to mimic. The chemical shifts of the other two boron atoms are similar to those of an arachno iridapentaborane with the metal in the apical position.[12]

Of course the assignment of **4-I** and **4-II** could be reversed; however, the essential fact remains. The new product is an arachno diruthenapentaborane. Is **4-II** reasonable considering that this structural type is not found in pure borane chemistry? A nido to arachno structural transformation similar to (b) has been observed in pure metal cluster chemistry upon addition of a two-electron ligand to a 7-sep square pyramidal cluster.[21,22] Considering the fact that **4** is 40% metal and 60% borane, it is reasonable that characteristics of the metal systems are competitively displayed. In addition,

(20) Boocock, S. K.; Toft, M. A.; Inkrott, K. E.; Hsu, L.-Y.; Huffman, J. C.; Folting, K.; Shore, S. G. *Inorg. Chem.* **1984**, *23*, 3084.
(21) Johnson, B. F. G.; Lewis, J.; Nicholls, J. N.; Puga, J.; Whitmire, K. H. *J. Chem. Soc., Dalton Trans.* **1983**, 787.
(22) Johnson, B. F. G.; Lewis, J.; Nicholls, J. N.; Puga, J.; Raithby, P. R.; Rosales, M. J.; McPartlin, M.; Clegg, W. *J. Chem. Soc., Dalton Trans.* **1983**, 277.

the existence of isomeric cluster structures is not uncommon in metal cluster chemistry.[23,24]

Finally, **4** is not produced by the reaction of free CO with **1**. As with $Cp^*Co(CO)B_3H_7$[25] and $Cp^*Ir(CO)B_3H_7$[12] found in reactions of other metallaboranes with $Co_2(CO)_8$, the presence of $Co_2(CO)_8$ is required for the formation of **4**. Presumably an intermediate species containing a cobalt carbonyl fragment loses a $Co(CO)_x$ fragment, leaving one or more CO ligands behind.

Isolation and Characterization of $\{Cp^*Ru(CO)_2\}Co(CO)_4$. A significant fraction of the reaction mixture consists of $\{Cp^*Ru(CO)_2\}Co(CO)_4$, and it was isolated and structurally characterized. During the course of this work the structure was published by others.[26] The η^5-C_5H_5 derivative is also known.[27]

Time Dependence of Product Distribution. ^{11}B and ^1H NMR studies of the reaction of **1** with $Co_2(CO)_8$ were carried out for a variety of reactant stoichiometries and concentrations. Results of two such runs, shown in Figures 3 and 4 (Supporting Information), illustrate the behavior observed. The ^{11}B spectra were integrated relative to a constant external reference of $[B_3H_8]^-$, and as shown by the boron balance, products **2**−**4** constitute better than 95% of the boron originally in **1**. **2** is the major product, whereas, under these conditions of less than stoichiometric $Co_2(CO)_8$ concentration and benzene solvent (see below), yields of **3** and **4** are about the same. **1** is largely consumed in the first 25 min of reaction, after which the system reaches an approximately stationary state. This plateau region is used below to evaluate the dependence of product yield on stoichiometry.

The decay of **1** is better illustrated in the early time data for the ^1H NMR experiment in Figure 4 (Supporting Information). These Cp* intensities measure the change in Cp*Ru fragments during the course of the reaction, and the products plotted constitute better than 85% of the initial Cp*Ru content of **1**. By comparison of the intensities of **2** and **4** in the ^1H and the ^{11}B spectra, it is clear that the relative yields of these products in the stationary state region are similar for the two differing reactant stoichiometries. The relative yield of **3**, however, decreases by a factor of ≈3 (25 vs 7%) on going from $Co_2(CO)_8$/**1** of 0.31 to 0.61. This corroborates the earlier study in which the yield of **3** is found to be improved at low $Co_2(CO)_8$ levels.

Another non-boron-containing product that was measured is $HCo(CO)_4$, and its time evolution at various $Co_2(CO)_8$/**1** stoichiometries is illustrated in Figure 5 (Supporting Information). At low $Co_2(CO)_8$/**1** small amounts of $HCo(CO)_4$ are found with the time behavior of an intermediate; that is, it is formed and then consumed under the reaction conditions. Presumably, $HCo(CO)_4$ is converted into H_2 and $Co_2(CO)_8$, and the latter reenters the reaction manifold. A maximum in $HCo(CO)_4$ is evident at higher $Co_2(CO)_8$/**1**; however, complete consumption is not observed in the time period observed. At the highest $Co_2(CO)_8$/**1** $HCo(CO)_4$ is simply one of the primary products. $Co_4(CO)_{12}$ is a product of this reaction at high $Co_2(CO)_8$/**1**; however, there was no convenient way of measuring it as a function of time.

Reaction Stoichiometry. A series of reactions were examined with ^1H NMR for $Co_2(CO)_8$/**1** ratios ranging from 0.2 to 2.4 as well as for several concentrations at fixed $Co_2(CO)_8$/**1**. These data add more detail to the basic observations described in the last section. In all cases the composition data used are taken from the near stationary state region of plots similar to Figure 4 (Supporting Information). Differences in reagent concentration at fixed $Co_2(CO)_8$/**1** had no statistically significant effect on product distribution in this region.

In Figure 6 (Supporting Information), the plot of overall loss of starting material as a function of $Co_2(CO)_8$/**1** shows that at $Co_2(CO)_8$/**1** ≈ 0.5 all of **1** is consumed. Figure 7 (Supporting Information) shows that the half-life of **1** depends strongly on $Co_2(CO)_8$/**1**. The data were not sufficiently precise to be used to define a reaction order, and given the established complex rate behavior of reaction systems involving $Co_2(CO)_8$,[28] it was not judged worthwhile obtaining this information.

The overall yield of **2** was 35−40%. The ratio **4**/**2** ranged from 0.5−0.8 based on Cp* integration (9 determinations), BHB integration (9 determinations), and ^{11}B integration (4 determinations). The ratio $\{Cp^*Ru(CO)_2\}Co(CO)_4$/**2** ranged from 0.3 to 0.5, Cp* integration (8 determinations), which is similar to the isolated yield. As already mentioned, the yield of **3** depends on $Co_2(CO)_8$/**1**. The dependence of the ratio **3**/**4** on $Co_2(CO)_8$/**1** is illustrated in Figure 8 (Supporting Information). Although the relative yield of **3** decreases continuously with increasing $Co_2(CO)_8$/**1**, the dependence is decidedly stronger at $Co_2(CO)_8$/**1** < 0.5. Of course, under these conditions **1** is not completely consumed (Figure 6, Supporting Information), so the absolute yield of **3** is still not high.

Solvent Effect. As already mentioned, **4** is not a major product when the reaction is carried out in hexane. Two major metallaborane products were isolated in the earlier work, **2** in 60% and **3** in 26% (but variable) yields, but only low abundances of **4** were seen in the NMR of reaction mixtures after **4** had been characterized. To obtain consistent data, a comparison of the relative product distribution in benzene, toluene, THF, and hexane was carried out for reactions with identical $Co_2(CO)_8$/**1** ratios and using ^1H NMR in the Cp* region to obtain yields. The results given in Figure 9 (Supporting Information) confirm the qualitative observations. Benzene and toluene exhibit similar product distributions, as expected. With THF the absolute yields of **2**−**4** are lower, but the relative yields are similar to those for benzene. However, the presence of increased amounts of the mixed metal complex, ruthenocene, and the ruthenium dimer suggests significant degradation during the reaction. In hexane, **2** and **3** have abundances similar to those in benzene, but that of **4** is considerably lower. Again it is an increase in degradation products that accounts for the low amount

(23) Cowie, A. G.; Johnson, B. F. G.; Lewis, J.; Raithby, P. R. *J. Organomet. Chem.* **1986**, *306*, C 63.
(24) Conole, G.; McPartlin, M.; Powell, H. R.; Dutton, T.; Johnson, B. F. G.; Lewis, J. *J. Organomet. Chem.* **1989**, *379*, C1.
(25) Lei, X.; Shang, M.; Fehlner, T. P. *Organometallics* **1998**, *17*, 1558.
(26) Matsuzaka, H.; Ichikawa, K.; Ishioka, T.; Sata, H.; Okubo, T.; Ishii, T.; Yamashita, M.; Kondo, M.; Kitagawa, S. *J. Organomet. Chem.* **2000**, *596*, 121.
(27) Manning, A. R. *J. Chem. Soc., A* **1971**, 2321.
(28) Absi-Halabi, M.; Atwood, J. D.; Forbus, N. P.; Brown, T. L. *J. Am. Chem. Soc.* **1980**, *102*, 6248.

Chart 3

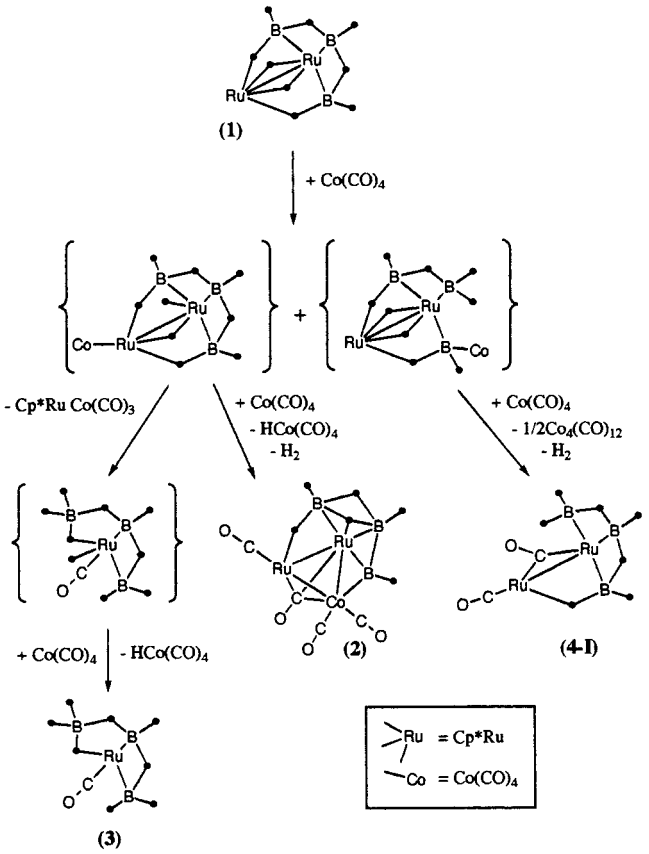

of **4** observed. The increase in $[Cp^*Ru(CO)_2]_2$ in hexane is particularly significant, as several attempts to crystallize **4** resulted in crystals of this degradation product. These observations suggest an intermediate in the formation of **4**, but not **2** and **3**, does not survive in hexane.

Summary

Previously we have observed metal fragment addition to a metallaborane, metal fragment substitution, and metal fragment elimination coupled with CO addition. The generation of **4** resulting from $Co_2(CO)_8$-promoted addition of CO combined with ruthenium fragment retention is new. Not only is the reaction pathway new but the product is a new metallaborane structure type—a dimetallapentaborane-11, which can adopt energetically similar borane-like (**4-I**) and metal cluster-like geometries (**4-II**). Although we have no quantitative mechanistic information, a reasonable pathway to explain the complex reaction of **1** with $Co_2(CO)_8$ can be postulated.

The presence of radicals in the chemistry of $Co_2(CO)_8$ is well established, and several studies have implicated their presence in metal cluster chemistry.[29] We have provided circumstantial evidence for their presence in the reactions of metallaboranes with $Co_2(CO)_8$.[25,30] Hence, it is likely that in this system the chemistry features a prominent role for the $Co(CO)_4$ radical. Thus, we postulate the reaction pathway given in Chart 3. In parallel reactions $Co(CO)_4$ radical addition generates a metal-based radical and a boron-based radical. The former undergoes unimolecular elimination of a mixed metal fragment (that leads to $\{Cp^*Ru(CO)_2\}Co(CO)_4$) leading to **3** in competition with H abstraction by $Co(CO)_4$ leading to **2**. Hence, at low $Co_2(CO)_8$/**1**, **3** should be favored at the expense of **2**. The boron-based radical undergoes $Co(CO)_4$ addition and $Co_2(CO)_6$ elimination (that generates $Co_4(CO)_{12}$), thereby leading to **4**. As **2** and **4** have the same dependence on cobalt fragment concentration, their abundances are determined by the relative abundances of the two, first-formed radical intermediates in a given solvent.

The apparent solvent dependence, particularly the low yield of **4** in hexane, is difficult to understand, but we can offer the following tentative explanation. It is known that the presence of small amounts of oxygen affects rates of reactions involving $Co_2(CO)_8$[28] and can even completely change the products observed.[31] Consequently, we postulate that the boron-centered radical may be much more sensitive to impurities, e.g., oxygen, than is the metal-centered radical. What is not understood is why hexane should be special. Given that relatively small rate differences in a competitive reaction system would account for the observations, the ultimate origin of the solvent dependence remains obscure.

Experimental Section

General Procedures. Standard Schlenk techniques were used.[32] Solvents were distilled immediately before use under N_2:sodium benzophenone ketyl for hexanes and tetrahydrofuran and molten sodium metal for toluene. Benzene-d_6 and toluene-d_8 were dried and stored over potassium metal mirrors in Young's tube and degassed using a freeze−thaw process. $(Cp^*Ru)_2B_3H_9$ was synthesized according to the literature.[11] $[Cp^*RuCl_2]_2$ and $Co_2(CO)_8$ (Strem) were used as received for synthesis, but for the NMR study, $Co_2(CO)_8$ was recrystallized from hexane. 60−200-mesh silica gel (J. T. Baker) and 230−400-mesh silica gel (EM Science) were predried at 140 °C overnight before use. NMR references: internal (C_6D_6, δ_H 7.15 ppm) for ^1H; internal (C_6D_6, δ_C 128.0 ppm) for ^{13}C; external ($[(Me_4N)(B_3H_8)]$ in acetone-d_6, δ_B −29.7 ppm) for ^{11}B. Mass spectra: FAB in a 3-nitrobenzyl alcohol matrix.

Synthesis of 1,2-$\{Cp^*Ru\}_2(CO)_2B_3H_7$ (4). In a typical reaction, 200 mg (0.39 mmol) of $(Cp^*Ru)_2B_3H_9$ was loaded into a 200 mL round-bottom Schlenk-type flask fitted with a rubber septum cap, along with a magnetic stir-bar. About 150 mg (0.44 mmol) of $Co_2(CO)_8$ was then added dry to the flask. The flask was evacuated and charged with argon. Distilled toluene (20 mL) was added via syringe and the mixture sonicated briefly. After stirring for 1 h at room temperature, the toluene was removed in vacuo, and 10 mL of freshly distilled hexanes was added and removed under vacuum. The dry sample was dissolved in 10 mL of hexanes, and column chromatography (2 cm × 10 cm) was performed using 60−200-mesh silica gel as the stationary phase and 25% toluene/75% hexanes v/v as the initial mobile phase. Following complete elution of the minor products, the major reaction product, $(Cp^*Ru)_2B_3H_6Co(CO)_4$, and **4** were removed from the column as one band using freshly distilled diethyl ether. The ether was removed in vacuo, and the mixture of products was redissolved in 10 mL of hexanes. A second column was performed (2 cm × 7 cm) using 230−400-mesh silica gel as the stationary phase and 25%

(29) Horwitz, C. P.; Holt, E. M.; Shriver, D. F. *Organometallics* **1985**, *4*, 1117.
(30) Jun, C.-S.; Bandyopadhyay, A. K.; Fehlner, T. P. *Inorg. Chem.* **1996**, *35*, 2189.
(31) Absi-Halabi, M.; Brown, T. L. *J. Am. Chem. Soc.* **1976**, *99*, 2982.
(32) Shriver, D. F.; Drezdzon, M. A. *The Manipulation of Air-Sensitive Compounds*, 2nd ed.; Wiley-Interscience: New York, 1986.

toluene/75% hexanes v/v as the initial mobile phase. Complete elution of the major product, $(Cp^*Ru)_2B_3H_6Co(CO)_4$, which is a dark brown to black band on the column, was achieved with the initial solvent mixture. **4**, which is red-brown in color, was stripped off the column using diethyl ether. Isolated yield of the new product was ~15%. X-ray quality crystals were obtained by leaving a saturated toluene solution at −40 °C for 72 h.

Spectroscopic Data for 4-I. MS (FAB^+): $P^+ = 570$ *m*/*z* for $^{12}C_{22}{}^1H_{37}{}^{11}B_3{}^{16}O_2{}^{102}Ru_2$; calculated weighted average for all isotopomers lying within the instruments resolution, 570.1149 *m*/*z*; measured 570.1144 *m*/*z*. NMR: ^{11}B (^1H = 300 MHz) (hexane, 21 °C, δ), 37.0 (d, J_{B-H} = 110 Hz; {^1H}, s, 1B), −0.2 (m; {^1H}, s, 2B); ^1H (400 MHz) (C_6D_6, 21 °C, δ), 4.93 (partially collapsed quartet, pcq, 1H, B-H_t), 2.93 (pcq, 2H, B-H_t), 2.19 (pcq, 1H, B-H_t), 1.73 (s, 15H, C_5Me_5), 1.55 (s, 15H, C_5Me_5), −1.72 (s, br, 1H, B-*H*-B), −4.65 (s, br, 1H, Ru-*H*-B), −12.04 (s, br, 1H, Ru-*H*-B); ^{13}C {^1H = 600 MHz} (C_6D_6, 21 °C, δ), 228.7 (s, 2C, *C*═O), 97.6 (s, 5C, C_5Me_5), δ 96.4 (s, 5C, C_5Me_5), 10.1 (s, 5C, C_5Me_5), δ 10.0 (s, 5C, C_5Me_5). IR (KBr, cm^{-1}): 2490 w, 2417 w (B−H); 1948 s, 1816 s (C═O).

Spectroscopic Data for 4-II (in a mixture with 4-I). NMR: ^{11}B (^1H = 300 MHz) (hexane, 21 °C), 29.9 (1B), δ 1.5 (1B), −1.9 (1 B); ^1H (400 MHz) (C_6D_6, 21 °C), 1.78 (s, 15H, C_5Me_5), 1.52 (s, 15H, C_5Me_5), −1.7 (s, br, 1H, B-*H*-B), −4.7 (s, br, 1H, Ru-*H*-B), −11.4 (s, br, 1H, Ru-*H*-B). IR (KBr, cm^{-1}): 1923 m, 1750 m (C═O).

Synthesis of {Cp*Ru(CO)$_2$}Co(CO)$_4$. To a solution of $\{\eta^5\text{-}C_5Me_5Ru\}_2B_3H_9$ (0.350 g, 0.68 mmol) in 20 mL of hexane was dropwise added $Co_2(CO)_8$ (0.23 g, 0.68 mmol) in 20 mL of hexane. The reaction mixture was stirred for 1 h at 60 °C. Column chromatography was performed at room temperature. Elution with hexane gave a brown solution and then with ether afforded **2**. The brown solution was kept at −40 °C overnight. Orange crystals were collected by filtration. The mother solution was concentrated and kept at −40 °C. The second crop of orange crystals was produced and collected. The orange crystals are highly soluble in hexane. The yield is ~22% (70 mg) based on the Ru.

Spectroscopic Data for {(η^5-C$_5$Me$_5$)Ru(CO)$_2$}(μ-CO)Co(CO)$_3$. MS (EI), P^+ = 464, 1Ru atom. Calcd for weighted average of isotopomers lying within the instrument resolution, 463.9237, obsd, 463.9205. NMR: ^1H (C_6D_6, 22 °C, δ), 1.39 (s, C_5Me_5), ^{13}C (C_6D_6, 22 °C, δ), 208.3 (s, CO), 101.5(s, C_5Me_5), 10.0(s, C_5Me_5). IR (hexane, cm^{-1}): 2059 s, 2009 s, 1979 s, 1826 m (CO). Anal. Calcd for $C_{16}H_{15}O_6RuCo$: C, 41.48; H, 3.26. Found: C, 41.60; H, 3.09.

X-ray Structure Determinations of 1,2-{Cp*Ru}$_2$(CO)$_2$B$_3$H$_7$ (4). An orange-red needle of $(Cp^*Ru)_2B_3H_9(CO)_2$ was mounted on a glass fiber for X-ray crystallographic analysis. Intensity data were measured at 293 K on an Enraf-Nonius CAD4 diffractometer equipped with a fine focus Mo-target X-ray tube (λ = 0.71073 Å) and powered at 55 kV and 32 mA. Most of the non-hydrogen atoms were located by the direct method. The remaining non-hydrogen atoms were found in succeeding difference Fourier synthesis. Least-squares refinement was carried out on F^2 for all reflections. After all non-hydrogen atoms were refined anisotropically, difference Fourier synthesis located the hydrogen atoms, which included the Cp* hydrogen atoms and the terminal and bridging borane hydrogen atoms. In future refinements a riding model was applied and the thermal parameters were assigned as 120% of the atom to which they were bonded. All reflections, including those with negative intensities, were included in the refinement. Crystal data and information on structure refinement are given in Table 1.

Table 1. Crystal Data and Structure Refinement for 1,2-{Cp*Ru}$_2$(CO)$_2$B$_3$H$_7$ (4)

empirical formula	$C_{22}H_{37}B_3O_2Ru_2$
fw	568.09
cryst habit	monoclinic
space group	*P*2(1)/*c*
unit cell dimens	*a* = 14.5880(10) Å *b* = 14.3512(10) Å *c* = 24.1283(10) Å α = 90° β = 104.230(10)° γ = 90°
volume	4896.4(5) Å^3
Z	8
density (calcd)	1.541 Mg/m^3
F(000)	2304
wavelength	0.71073 Å
abs coeff	1.248 mm^{-1}
cryst size	0.45 × 0.12 × 0.10 mm^3
temperature	293(2) K
diffractometer	Enraf-Nonius CAD4
θ range for data collection	2.01−24.99°
index ranges	$0 \le h \le 17$, $0 \le k \le 17$, $-28 \le l \le 27$
total data collected	8951
unique data	8600 [*R*(int) = 0.0836]
abs corr	semiempirical
max. and min. transmn	0.8960 and 0.6970
refinement method	full-matrix least-squared on F^2
no. of data/restraints/params	8600/0/526
goodness-of-fit on F^2	1.103
final *R* indices [$I > 2\sigma(I)$]	R1 = 0.0607, wR2 = 0.1563
R indices (all data)	R1 = 0.1509, wR2 = 0.1763
largest diff peak and hole	1.501 and −1.688 e·Å^{-3}

NMR Study. In a typical reaction, 25 mg (0.048 mmol) of **1** was weighed out in a 5 mm NMR tube. Recrystallized $Co_2(CO)_8$ was weighed in the same NMR tube at near the desired $Co_2(CO)_8$:$(Cp^*Ru)_2B_3H_9$ ratio. The NMR tube with the solid reagents was connected to a Schlenk line, evacuated, and filled with argon. A 0.7 mL sample of benzene-d_6 was added to the NMR tube to dissolve the solid reagents and to provide a lock and reference signal for the NMR experiment. The NMR tube was capped with a rubber septum, inverted several times, and sonicated briefly to ensure a homogeneous mixture and then frozen in liquid N_2 to stop the reaction. At the spectrometer, the NMR tube was warmed by hand to room temperature and placed in the spectrometer. The reactions were monitored via ^1H NMR at 500 MHz employing a preacquisition delay. A new free induction decay (FID) was taken every minute for the first 20 min, every 5 min for the following 100 min, and one FID after 3 h total. The acquisition time for one FID was 1 min. The Cp* and hydride regions were integrated separately.

Acknowledgment. We thank Dr. Maoyu Shang and Dr. Alicia M. Beatty for the X-ray structure determination of **4**. We are grateful to the National Science Foundation and The Petroleum Research Foundation administered by the American Chemical Society for the financial support of this research.

Supporting Information Available: A listing of tables of crystal data, atomic coordinates and isotropic displacement parameters, bond lengths and angles, and anisotropic displacement parameters for **4**, as well as Figures 3−9. This material is available free of charge via the Internet at http://pubs.acs.org.

OM010589Q